

Performance Analysis of Energy Pattern and Power Patterns for UWB Antenna and Narrowband Antenna

Dau-Chyrh CHANG^{†a)}, Chao-Hsiang LIAO^{††}, and Powen HSU^{††}, *Nonmembers*

SUMMARY Power patterns in the frequency domain are usually used to describe the antenna performance in narrowband communication systems; however, they are not sufficient for ultra wideband (UWB) antennas in wideband communication systems. In this paper, energy pattern and energy gain are introduced to describe the performance of UWB antennas. Numerical simulations and measurements are used to demonstrate the difference between power patterns and energy patterns for narrowband Yagi-Uda antenna, UWB CPW-fed bow-tie slot antenna, and UWB comb taper slot antenna. The results of simulations and measurements are agreement not only in energy pattern, but also in received voltage at various observation angles. For narrowband antennas, the energy patterns are similar to that of the power patterns in the main beam region. However, there are quite differences between power pattern in frequency domain and energy pattern in time domain for UWB antennas.

key words: energy pattern, energy gain, power pattern, ultra wideband (UWB) antenna

1. Introduction

In general the parameters of antennas are characterized by input impedance, efficiency, gain, directivity, effective area, radiation pattern, beamwidth, polarization properties, etc. [1]. It is well known that antenna parameters are function of the frequency. For narrowband applications it is possible to analyze these parameters within the narrow band. For wider bandwidths, antenna parameters change greatly from frequency to frequency. The parameters as functions of frequency are not sufficient for the characterization of the communication system.

The UWB antenna, which has a frequency bandwidth of more than 100%, has been studied extensively [2]–[4]; Thus, the frequency domain concepts and terminology commonly used to describe power patterns of narrowband antennas may not be suitable for the UWB antenna. Traditionally, the antenna power pattern in the frequency domain is the spatial variation of the radiation intensity along a constant radius. On the other hand, although the UWB antenna includes the capability of processing ultra wideband spectrum, the power patterns in frequency domain of the UWB antenna will be different from frequency to frequency. If the UWB antenna is defined as the energy pattern in the time-

domain instead of power pattern in frequency domain, the complex pattern will be solved easily. The energy pattern of the antenna is the total response of the power patterns in the frequency domain. This provides a simple representation of antenna behavior as that of a large number of power patterns. If using the proposed solution for UWB antenna, it is easier to describe the performance of UWB antenna.

In order to provide more insight and more effective terminology for UWB antennas, the energy pattern of antennas will be analyzed by using the received voltage or electric field intensity. In order to verify the results of simulation, antenna energy patterns are also measured. In this paper, the power pattern, power gain, energy pattern, and energy gain of narrowband and UWB antennas were simulated and measured. These verified antennas will include Yagi-Uda antenna, UWB CPW-fed bow-tie slot antenna, and UWB comb taper slot antenna.

2. Formulation of the Energy Pattern

The energy pattern $U_E(\theta, \phi)$ at direction (θ, ϕ) in the time domain was defined in Refs. [5]–[7] and is given in Eq. (1):

$$U_E(\theta, \phi) = \frac{1}{\eta_0} \int_{-\infty}^{+\infty} |\bar{E}_{rad}(t, R, \theta, \phi)|^2 R^2 dt \quad (1)$$

The energy pattern can also be verified in the frequency domain as shown in Eq. (2):

$$U_E(\theta, \phi) = \frac{1}{2\pi\eta_0} \int_{-\infty}^{+\infty} |\bar{e}_{rad}(\omega, R, \theta, \phi)|^2 R^2 d\omega \quad (2)$$

where η_0 is the intrinsic impedance of free space (377 ohm), and $\bar{E}_{rad}(t, R, \theta, \phi)$, $\bar{e}_{rad}(\omega, R, \theta, \phi)$ are the radiated electric field intensity in the time domain and in the frequency domain, respectively. Although the electric field intensity depends on the range R , the energy pattern will not depend on the range R . The unit of power pattern is in watt per unit solid angle, while the unit of energy pattern is in joule per unit solid angle.

The energy pattern indicates the value of energy intensity received or radiated by the antenna. The energy pattern at the (θ, ϕ) direction is the energy per unit solid angle radiated by the antenna integrated over the whole time domain, which represents the time waveform of the detected energy intensity, as a function of the direction of the incident signal.

Usually the UWB time waveform envelops decay rapidly. In order to speed up the computation time, the energy pattern will be simulated or measured and time-gated

Manuscript received April 1, 2011.

Manuscript revised August 15, 2011.

[†]The author is with the Communication Research Center, Oriental Institute of Technology, Taipei, Taiwan, R.O.C. (Corresponding author.)

^{††}The authors are with the Department of EE, National Taiwan University, Taipei, Taiwan, R.O.C.

a) E-mail: dcchang@mail.oit.edu.tw

DOI: 10.1587/transcom.E95.B.2

over $[t_1, t_2]$. The energy pattern in the (θ, ϕ) direction can be modified as in Eq. (3):

$$U_E(\theta, \phi) = \frac{1}{\eta_0} \int_{t_1}^{t_2} |\bar{E}_{rad}(t, R, \theta, \phi)|^2 R^2 dt \quad (3)$$

The energy gain $G_E(\theta, \phi)$ is in time domain, which is analogous to the conventional power gain in frequency domain [8]–[13]. The energy pattern U_E can be normalized to the energy radiated by a hypothetical lossless, matched isotropic antenna driven by a source with the same available energy. The energy gain of an antenna is the product of overall energy efficiency and energy directivity as shown in Eq. (4):

$$\begin{aligned} G_E(\theta, \phi) &= \eta_E D_E(\theta, \phi) \\ &= \eta_E \frac{4\pi U_E(\theta, \phi)}{\int_0^{2\pi} \int_0^\pi U_E(\theta, \phi) \sin\theta d\theta d\phi} \end{aligned} \quad (4)$$

where D_E is the energy directivity. η_E is the total energy efficiency of the antenna, which is defined as the ratio of the total energy radiated to the total energy available at the antenna input as shown in Eq. (5):

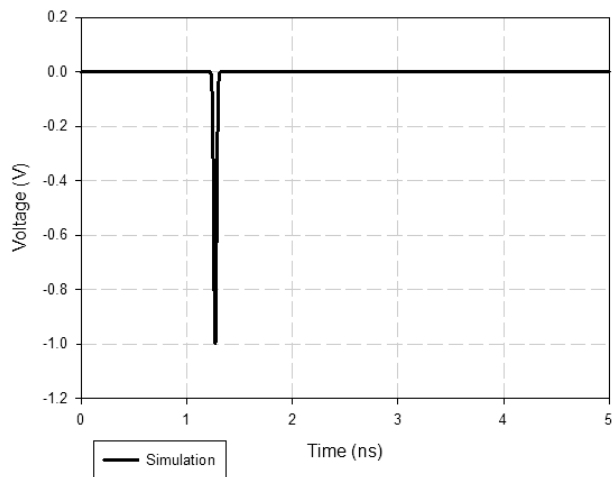
$$\eta_E = \frac{\int_0^{2\pi} \int_0^\pi \int_{t_1}^{t_2} |\bar{E}_{rad}(t, R, \theta, \phi)|^2 R^2 \sin\theta dt d\theta d\phi}{\eta_0 \int_{t_1}^{t_2} (V_S^2(t) / 4R_S) dt} \quad (5)$$

where V_S is the instantaneous source voltage and R_S is the source resistance.

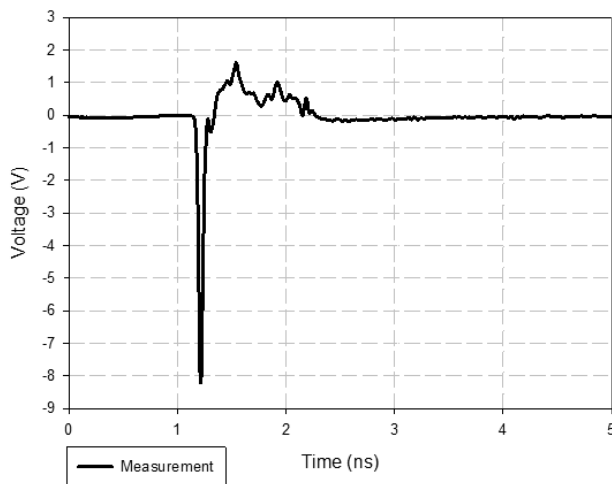
3. Response of Waveform for Different Antennas

UWB antennas enable the transmission of impulse without distortion [14]. The response of the impulse waveform could be used as the performance of antenna. In this section, the waveform of an excitation pulse by simulation and measurement and its spectrum will be discussed. The ideal Gaussian pulse as shown in Fig. 1(a) is used for simulation in this paper. The measurement impulse which from trigger generator is a similar to that of Gaussian pulse with pulse with 30 ps and amplitude 20 V. The receiver is a wideband digital sampling oscilloscope. The output impedance for the trigger generator and digital sampling oscilloscope are 50 ohm. Figure 1(b) is the measured results with attenuator, SMA connectors, and cable loss from trigger generator. Minor differences between the simulation and measurement, may cause by narrowband SMA connectors. Figure 1(c) is the comparison of normalized spectrum for both simulation and measurement. Since the higher the frequency the higher the losses for the SMA connector and the RF cable will be, the measurement result of spectrum decay rapidly for higher frequency, as shown in Fig. 1(c).

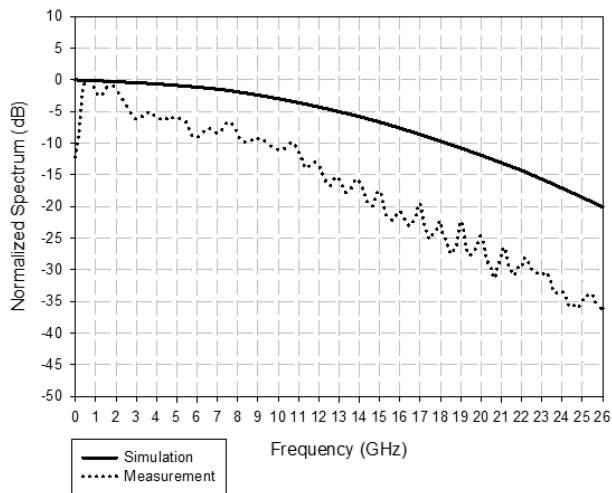
The simulation result is the electric field intensity (volt/meter) in the far-field region. The far field is simulated with a perfect source excitation delivering a Gaussian pulse at antenna input port. The measurement is performed with the same Gaussian pulse voltage source exciting a double ridge horn as the transmission antenna and the antenna



(a) Simulation waveform



(b) Measurement waveform



(c) Spectrum

Fig. 1 Waveform of excitation pulse by simulation (a) and measurement (b), and its spectrum (c).

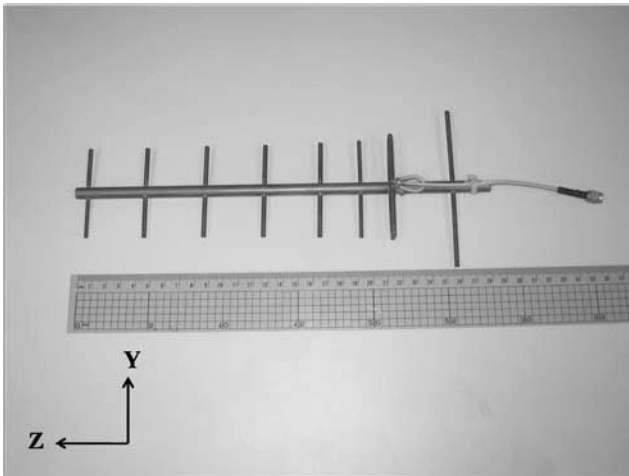


Fig. 2 Yagi-Uda antenna.

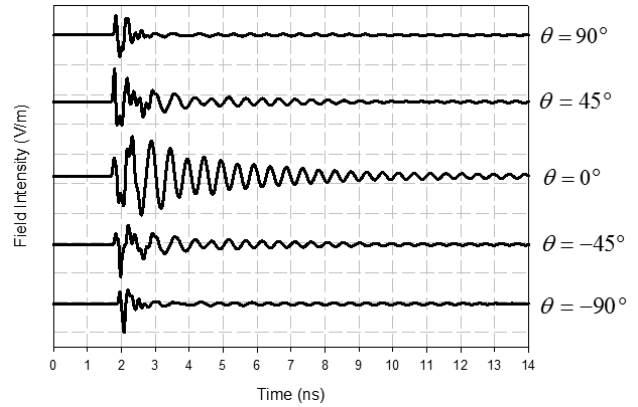
under test (AUT) is used as the receiving antenna. The measurement result is the voltage amplitude (volt) at the display of digital sampling oscilloscope. The time-domain response for narrowband Yagi-Uda antenna, UWB CPW-fed bow-tie slot antenna, and UWB comb taper slot antenna will be compared.

3.1 Yagi-Uda Antenna

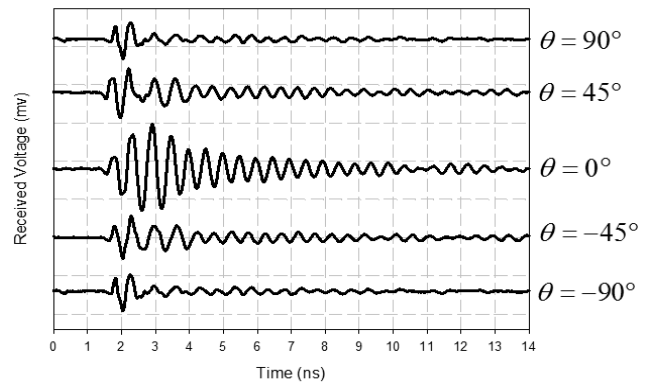
A typical eight-element Yagi-Uda antenna is shown in Fig. 2. It consists of a driven element (folded $\lambda/2$ dipole) fed by a balun, a reflector, and six directors. The size of antenna is 28 cm by 11 cm and its operating frequency bandwidth is from 1.75 GHz to 1.95 GHz. Figure 3 shows the time domain response of simulated field intensity and measured voltage of H-plane Yagi-Uda antenna at $\pm 45^\circ$, $\pm 90^\circ$, and endfire directions. The time signal converges slowly due to the narrow bandwidth. The results in time domain response from both simulation and measurement are very similar.

3.2 UWB CPW-Fed Bow-Tie Slot Antenna

UWB CPW-fed bow-tie slot antenna is shown in Fig. 4, which is fabricated on a 4.7 cm by 3.6 cm Rogers RO4003 substrate [15]. The RO4003 parameters are with relative permittivity 3.38, thickness 0.508 mm, and loss tangent 0.0027. The antenna structure is composed of a linear tapered transition slot line between the feeding CPW and the bow-tie slot antenna. By using this linear tapered transition, a 120% impedance bandwidth with 10 dB return loss is obtained. The consistency of the radiated pulse shape is a critical issue in UWB antenna performance for omnidirectional pattern [16]. Figure 5 shows the time domain response of simulated field intensity and measured voltage in the H-plane of the antenna at 0° , 45° , 90° , 135° , and 180° directions. From the results of Fig. 5, time waveform convergence is fast. The impulse time response is not sensitive to



(a) Simulation



(b) Measurement

Fig. 3 Comparison of the time domain response of simulated field intensity and measured voltage of Yagi-Uda antenna at 0° , $\pm 45^\circ$, and $\pm 90^\circ$ directions.

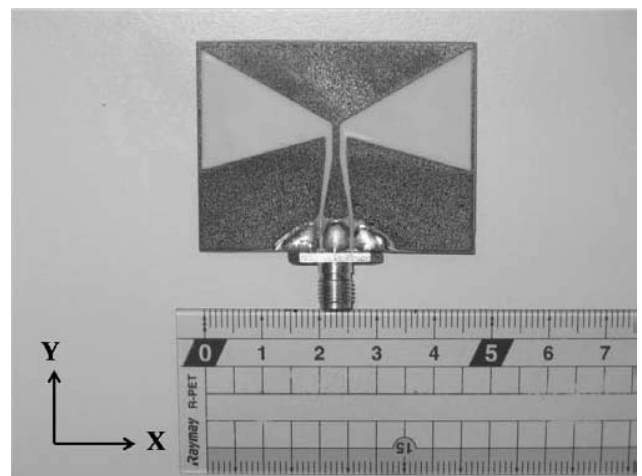
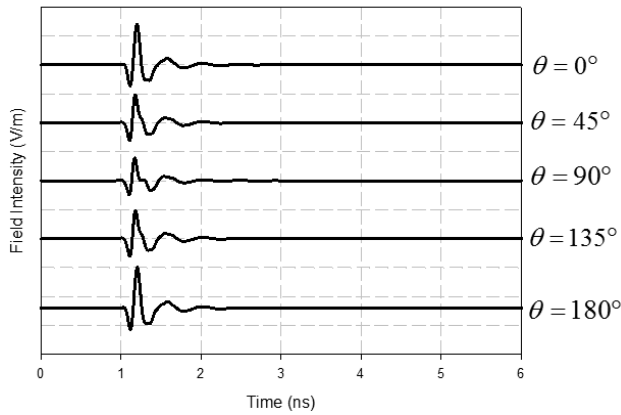
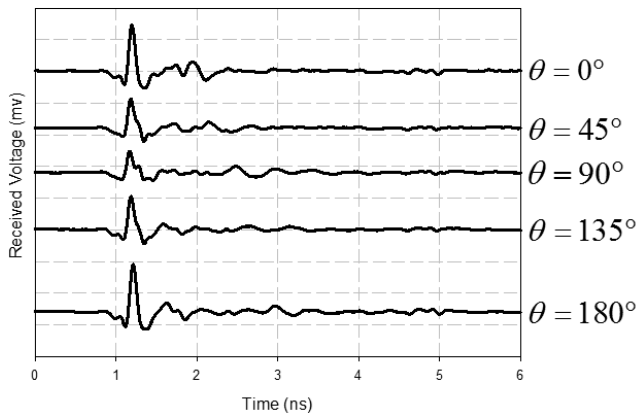


Fig. 4 UWB CPW-fed bow-tie slot antenna.

the direction of the incident wave. It shows that it is an omnidirectional UWB antenna. The minor difference is caused by the loss of SMA connectors and cable length.



(a) Simulation (10 mV/m/div for vertical axis)



(b) Measurement (10 mV/m/div for vertical axis)

Fig. 5 Comparison of the time domain response of simulated field intensity and measured voltage of CPW-fed bow-tie slot antenna at 0°, 45°, 90°, 135°, and 180° directions.

3.3 UWB Comb Taper Slot Antenna

UWB comb taper slot antenna [17], [18] is a UWB antenna as shown in Fig. 6. The antenna can achieve ultra wideband performance owing to its elegant transition from the microstrip line [19], [20]. The microstrip transition at the input is circularly tapered to parallel strips for the antenna feed. The antenna length is chosen according to the empirical guideline [21]. The taper flare is determined by using the recursive optimization of simulation software. The corrugations along the sides reduce the antenna width, improve the voltage standing wave ratio (VSWR) over a wide frequency range, and suppress the sidelobe levels [22]–[24]. The antenna is designed on a FR4 substrate with relative permittivity of 4.4, thickness of 0.8 mm, and loss tangent of 0.0254. The size of the antenna is 14 cm by 4 cm. Figure 7 shows the time response simulated field intensity and measured voltage in the H-plane at 0°, ±45°, and ±90° directions. The small ripple of the convergence for the test results may be caused by an imperfect of hardware imple-

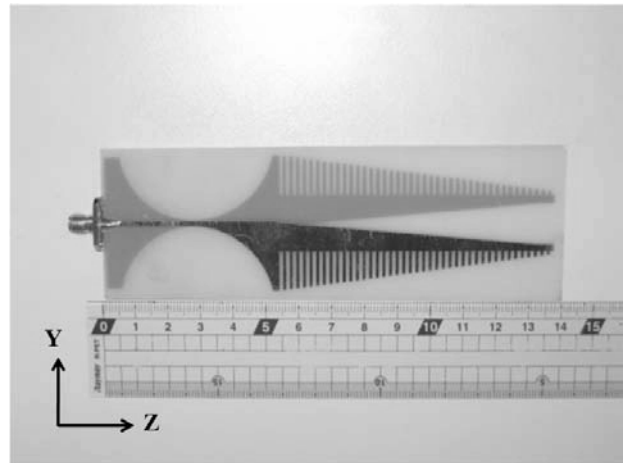
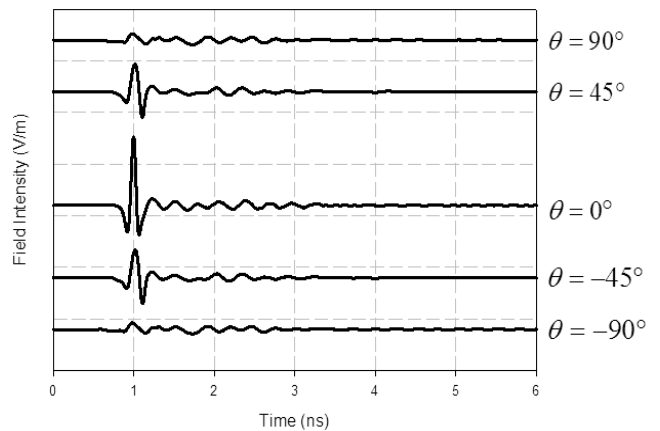
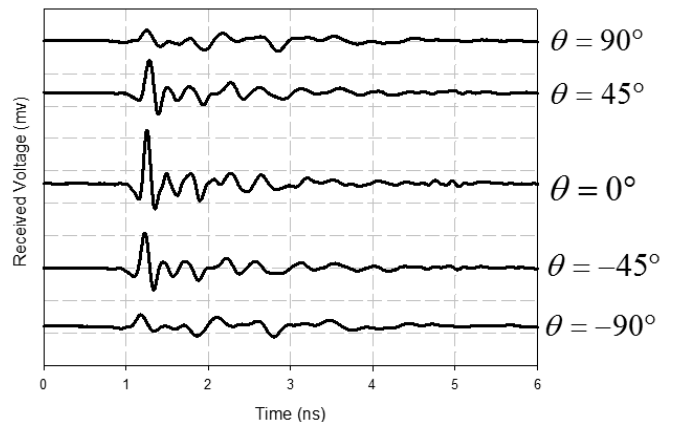


Fig. 6 UWB comb taper slot antenna.



(a) Simulation (10 mV/m/div for vertical axis)



(b) Measurement (10 mV/div for vertical axis)

Fig. 7 The time response of simulated field intensity and measured voltage of comb taper slot antenna at 0°, ±45°, and ±90° directions.

mentation. The voltage response is the maximum at the 0° endfire direction. The two beam minima occur at ±90° broadside directions. From these results, it is obvious that this is a directional UWB antenna.

4. Comparison of Energy and Power Patterns

Usually, the traditional vector network analyzer (VNA) will be capable of time domain measurements using software processing. It will take time for data transformation.

An impulse time domain antenna measurement system (ITDAMS) is the direct time domain antenna measurement method. It is not necessary to transform the received signal in the frequency domain into the time domain [25]. The direct method will save time during the voltage response measurement. The key components of ITDAMS are the commercially available trigger generator and receiver. The receiver is a wideband digital sampling oscilloscope. The receiver has an instantaneous bandwidth of 26 GHz and a linear dynamic range of 66 dB. The impulse signals received by the antenna under test (AUT) will include the desired signal and other undesired signals (fields from multiple bounces). The observation time window can be varied from 10 ps to 2000 ns with variable acquisition data points from 4 to 4096. If the observable multipath components are larger than that of time window, the variable range gate can adjust to select the desired signal from the complex incoming signals. The ITDAMS can also transform the gated received time signal into a frequency spectrum by using Fourier transformation.

The ITDAMS is used to measure both the energy pattern in the time domain and the power pattern in the frequency domain. The measured antenna patterns of the above three antenna examples will be compared.

Figure 8 shows the measured results of energy pattern and power patterns at 1.75 GHz, 1.85 GHz, and 1.95 GHz for the E- and H-planes of Yagi-Uda antenna. The energy patterns of Yagi-Uda antenna are quite similar to the power pattern in the main beam region. The sidelobe level of the energy pattern is higher than that of the power pattern. This is due to the residue of the time voltage response away from the broadside direction. The measured power gain is

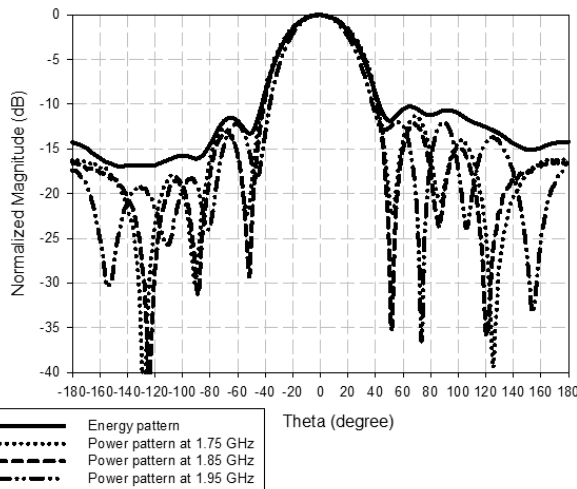


Fig. 8 Energy and power patterns in the H-plane of Yagi-Uda antenna. (X-Z plane)

around 10.3 dBi to 11.6 dBi within 1.75 GHz to 1.95 GHz. The measured energy gain in time domain is 10.83 dBi with gated time window 14 ns. The energy gain is quite similar to that of the power gain. Figure 9 shows the comparison of energy pattern in the H-plane by simulation and measurement. Except for the sidelobe level, the results of simulation and measurement are in good agreement.

Figure 10 shows the measurement results of energy pattern and power patterns at 4 GHz, 7 GHz, and 10 GHz for the H-plane of the UWB CPW-fed bow-tie slot antenna. The power patterns are quite different for these three frequencies. Figure 11 shows the comparison result of energy pattern in the H-plane by both simulation and measurement. The simulation and measurement results are in good agreement. The measured power gain varies from 2.52 dBi to 5.32 dBi for frequencies from 3.1 GHz to 10.6 GHz. However the measured energy gain in time domain is 3.19 dBi with gated time window 6 ns.

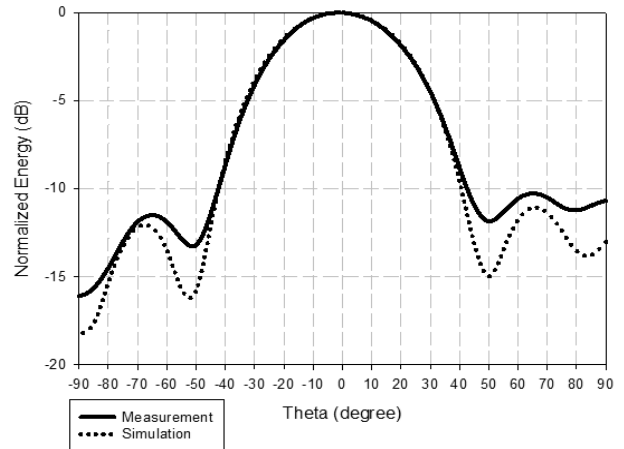


Fig. 9 Results of H-plane energy pattern of Yagi-Uda antenna by measurement and simulation. (X-Z plane)

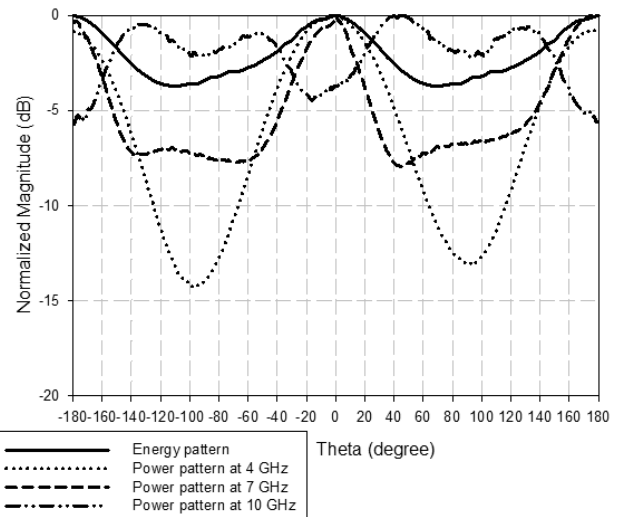


Fig. 10 Measurement results of H-plane energy and power patterns of CPW-fed bow-tie slot antenna. (X-Z plane)

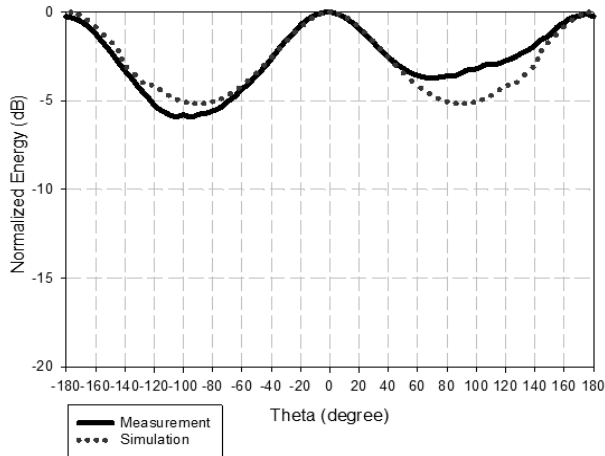


Fig. 11 Results of the H-plane energy pattern of CPW-fed bow-tie slot antenna by simulation and measurement. (X-Z plane)

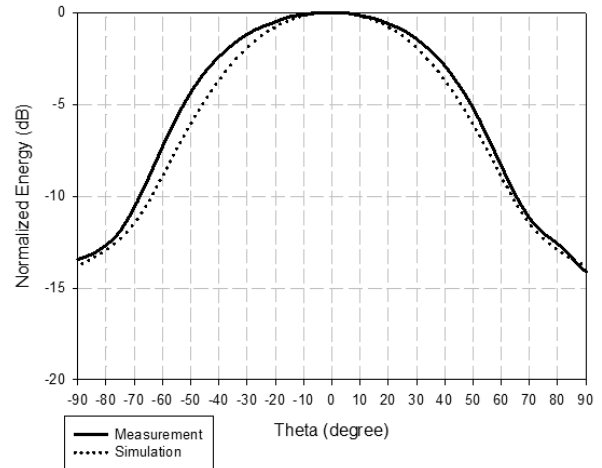


Fig. 13 Results of energy H-plane pattern of comb taper slot antenna by simulation and measurement. (X-Z plane)

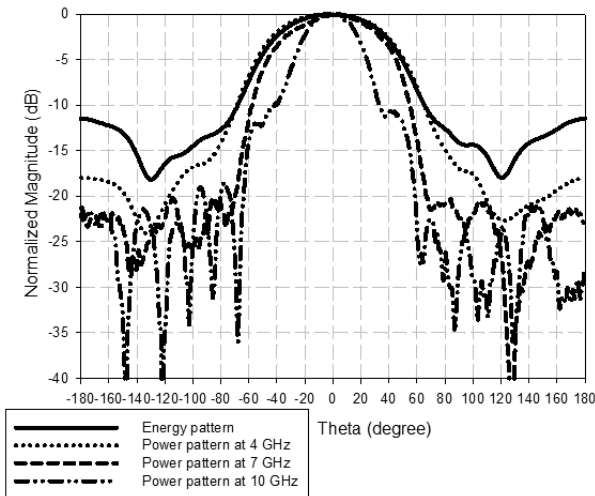


Fig. 12 Measurement results of H-plane energy and power patterns for comb taper slot antenna. (X-Z plane)

Figure 12 shows the measured results of energy pattern and power patterns at 4 GHz, 7 GHz, and 10 GHz in the H-plane of the UWB comb taper slot antenna. These power patterns are quite different for these three frequencies. Figure 13 shows the comparison result of the energy pattern by both simulation and measurement in the H-plane of this antenna. The results of simulation and measurement are quite similar. The variation of power gain is changed from 5.85 dBi to 10.32 dBi for frequencies from 3.1 GHz to 10.6 GHz. The measured energy gain in time domain is 7.38 dBi with gated time window 6 ns.

5. Conclusion

The time domain antenna parameters and their formulas have been presented. The time waveforms of narrowband and UWB antennas are quite different. For narrowband antennas, the convergence of the time response is very slow. For UWB antennas, the convergence of the time response is

very fast. In order to keep the maximum radiation energy, the time-gated $t_1 \sim t_2$ of a narrowband antenna should be wider than that of UWB antenna. The chosen of time window $t_1 \sim t_2$ will affect the energy pattern and energy gain. For omni-directional antennas, the impulse time response is independent of the direction of incident wave and it is almost the same at all directions. For directional antennas, the time response has a maximum at its beam’s maximum direction and minimum at its beam’s minimum direction. The simulated and measured energy patterns of three antennas have been compared. The results are in good agreement. For narrowband antennas, the power gain does not change too much inside the band. The energy pattern is similar to the power pattern in the main beam region and the energy gain is close to the power gain for narrowband antenna. For UWB antennas, the power patterns are quite different. The power gain and energy gain are also different.

Acknowledgments

This work was supported by the National Science Council, Taiwan (R.O.C.), under contract NSC 97-2221-E-161-003.

References

- [1] C.A. Balanis, *Antenna Theory, Analysis and Design*, Wiley, New York, 1997.
- [2] K.Y. Yazdandoost and R. Kohn, “Ultra wideband antenna,” *IEEE Commun. Mag.*, vol.42, pp.S29–S32, 2004.
- [3] T.G. Ma and S.K. Jeng, “Planar miniature tapered-slot-fed annular slot antennas for ultrawide-band radios,” *IEEE Trans. Antennas Propag.*, vol.53, no.3, pp.1194–1202, 2005.
- [4] Z.N. Chen, “Novel bi-arm rolled monopole for UWB applications,” *IEEE Trans. Antennas Propag.*, vol.53, no.2, pp.672–677, 2005.
- [5] J.S. McLean, H. Foltz, and R. Sutton, “Pattern descriptors for UWB antennas,” *IEEE Trans. Antennas Propag.*, vol.53, no.1, pp.553–559, 2005.
- [6] M.G.M. Hussain, “Antenna energy patterns of nonsinusoidal waveforms,” *IEEE Trans. Electromagn. Compat.*, vol.EMC-29, no.1, pp.24–31, 1987.

- [7] D. Lamensdorf and L. Susman, "Baseband-pulse-antenna techniques," *IEEE Antennas Propag. Mag.*, vol.36, no.1, pp.20–30, 1994.
- [8] E.G. Farr and C.E. Baum, "Extending the definitions of antenna gain and radiation pattern into the time domain," *Sensor Simulation Notes*, note 350, pp.1–43, 1992.
- [9] A. Shlivinski, E. Heyman, and R. Kastner, "Antenna characterization in the time domain," *IEEE Trans. Antennas Propag.*, vol.45, no.7, pp.1140–1149, 1997.
- [10] H. Schantz, *The Art and Science of Ultrawideband Antennas*, Artech House, 2005.
- [11] C. Roblin, S. Bories, and A. Sibille, "Characterization tools of antennas in the time domain," *IWUWBS*, Oulu, June 2003.
- [12] C. Roblin, "Ultra compressed parametric modeling for symmetric or pseudo-symmetric UWB antenna," *ICUWB*, Invited Papers on Ultrawideband Antennas, Hannover (Ger.), Sept. 2008.
- [13] C. Roblin and A. Sibille, "Ultra compressed parametric modeling of UWB antenna measurements using symmetries," 29th *URSI General Assembly*, Chicago, Aug. 2008.
- [14] Z.N. Chen, X.H. Wu, H.F. Li, N. Yang, and M.Y. W. Chia, "Considerations for source pulses and antennas in UWB radio systems," *IEEE Trans. Antennas Propag.*, vol.52, no.7, pp.1739–1748, 2004.
- [15] D.C. Chang, "UWB antennas and their applications," *Proc. iWAT2008*, pp.14–19, Chiba, Japan, March 2008.
- [16] D.M. Pozar, "Waveform optimization for ultrawideband radio systems," *IEEE Trans. Antennas Propag.*, vol.31, no.9, pp.2335–2345, 2003.
- [17] D.C. Chang, B.H. Zeng, and L.C. Liu, "Modified antipodal Fermi antenna with piecewise-linear approximation and shaped-comb corrugation for ranging applications," *IET Microw. Antennas Propag.*, vol.4, no.3, pp.399–407, 2010.
- [18] C.-H. Liao, D.-C. Chang, and P. Hsu, "Ultra-wideband antenna array by comb taper slot antenna," *Proc. International Symposium on Antennas and Propagation*, pp.1031–1034, Taipei, Taiwan, Oct. 2008.
- [19] E. Gazit, "Improved design of the Vivaldi antenna," *Proc. Inst. Elect. Eng.*, pt. H, vol.135, pp.89–92, April 1988.
- [20] S.G. Kim and K. Chang, "Ultrawide-band transitions and new microwave components using double-sided parallel-strips lines," *IEEE Trans. Microw. Theory Tech.*, vol.52, no.9, pp.2148–2152, 2004.
- [21] K.S. Yngvesson, "Endfire tapered slot antennas on dielectric substrates," *IEEE Trans. Antennas Propag.*, vol.AP-33, no.12, pp.1392–1400, 1985.
- [22] S. Sugawara, Y. Maita, K. Adachi, K. Mori, and K. Mizuno, "A mm-wave taper slot antenna with improved radiation pattern," *IEEE MTT-S Int. Microw. Symp. Dig.*, pp.959–962, 1997.
- [23] H. Sato, K. Sawaya, Y. Wagatsuma, and K. Mizuno, "Broadband FDTD analysis of fermi antenna with narrow width substrate," *IEEE AP-S Int. Symp.*, Dig., vol.1, pp.261–264, 2003.
- [24] H. Sato, K. Sawaya, Y. Wagatsuma, and K. Mizuno, "Design of narrow-width Fermi antenna with circular radiation pattern," *IEEE AP-S Int. Symp. Dig.*, vol.4, pp.312–315, June 2004.
- [25] D.C. Chang, C.H. Liao, and C.H. Wu, "CATR without both reflector edge treatment and RF anechoic chamber," *IEEE Antennas Propag. Mag.*, vol.46, no.4, pp.27–37, Aug. 2004.



Dau-Chyrh Chang was born in Taiwan. He obtained his B.S. degree and M.S. degree from Chung-Cheng Institute of Technology in 1970 and 1973, respectively, and Ph.D. degree in Electrical Engineering from University of Southern California in 1981. Prof. Chang spent 17 years (1981–1998) in antenna R&D at CSIST (Chung Shan Institute of Science and Technology). For 12 of these years (1986–1998), he served as the director of antenna section. During his employment at CSIST, he developed the

reflector antennas, phased array antennas, slot array antennas, and communication antennas. He also established the new and innovative antenna test ranges (near field range in 1986, and compact range in 1987) in Taiwan. In 1998, Prof. Chang left his post as the director of the antenna section to become the Dean of the Engineering School at Da-Yeh University. He had been invited to be the Dean of College of Electrical and Communication Engineering at Oriental Institute of Technology in 2006. Since then, his achievements have included: (1) Developments of hybrid near field and compact ranges for various kinds of antenna testing; (2) applications of impulse time domain system; (3) developments of various kinds of UWB antenna and smart antennas for communication system. He established the IEEE AP-S Taipei Chapter and as the first Chair in 2001, Chair of IEEE MTT-S Taipei Chapter (2000–2002), President of Chinese Microwave Association (2000–2002). He has been the General Chair of CSTRWC2001, CSTRWC2008, ISAP2008, ICONIC2009, AEM2C2010, and IEEE iWEM2011. He is the Chair Professor and Director of Communication Research Center at Oriental Institute of Technology. He is a Fellow of IEEE, IET, and EMA.



Chao-Hsiang Liao was born in Taipei, Taiwan. He received the B.S. and M.S. degrees in electrical engineering from Da Yeh University, Changhua, Taiwan, in 2002 and 2005, respectively, and the Ph.D. degree in communication engineering at National Taiwan University, Taipei, Taiwan, in 2010. From 2002 to 2005, he was with the Wireless Communication Research Center (WCRC), Da Yeh University, where he has been engaged in the analysis and design of reflector antennas, and also the development of

the Da Yeh University compact antenna test range (CATR). He has done considerable work on the optimum design of reflector antennas for DBS. From 2006 to 2010, he was with the Communication Research Center (CRC), Oriental institute of Technology, where he has been engaged in the performance analysis of UWB arrays with beam scan capability, and energy pattern of UWB antenna array for real beam radar imaging. His main research interests are optimum design of reflector antennas for direct broadcast satellite, design and analysis of UWB antennas, and high resolution microwave imaging for radar applications. He received the best student paper award from 2008 International Symposium on Antennas and Propagation (ISAP 2008), the third prize best paper award from 4th International Conference on Electromagnetic Near-Field Characterization and Imaging (ICONIC 2009), and the best paper award from 2010 International Conference on Applications of Electromagnetism and Student Innovation Competition Awards (AEM2C 2010).



Powen Hsu was born in Taipei, Taiwan. He received the B.S. degree in physics from the National Tsing-Hua University, Hsinchu, Taiwan, in 1972, the M.S. degree in physics from the University of Maryland, College Park, in 1976, and the M.S. and Ph.D. degrees in electrical engineering from the University of Southern California, Los Angeles, in 1978 and 1982, respectively. From 1982 to 1984, he was with ITT Gilfillan, Van Nuys, CA, where he was engaged in research and development pertaining to radar

antenna systems. In 1984, he joined the faculty of the National Taiwan University, Taipei, Taiwan, where he is currently a Professor with the Electrical Engineering Department. From 1992 to 1995, he was the Department Chairperson there. In August 1997, he established the ninth college, College of Electrical Engineering and Computer Science, in the National Taiwan University, and served as the first Dean of the College until 2003. His current research interests include the design and analysis of slot antennas, microstrip antennas, and microwave and millimeter-wave integrated circuits. Prof. Hsu is a Fellow of IEEE and a Distinguished Professor of National Taiwan University.